




The Major Hurdle for Effective Baculovirus Transduction into Mammalian Cells Is Passing Early Endosomes

Liangbo Hu,^{a,b} Yimeng Li,^{a,b} Yun-Jia Ning,^a  Fei Deng,^a Just M. Vlak,^c Zhihong Hu,^a Hualin Wang,^a Manli Wang^a

^aState Key Laboratory of Virology, Wuhan Institute of Virology, Chinese Academy of Sciences, Wuhan, People's Republic of China

^bUniversity of the Chinese Academy of Sciences, Beijing, People's Republic of China

^cLaboratory of Virology, Wageningen University and Research, Wageningen, The Netherlands

ABSTRACT Baculoviruses, although they infect insects in nature, can transduce a wide variety of mammalian cells and are therefore promising gene therapy vectors. However, baculovirus transduction into many mammalian cells is very inefficient, and the limiting stages and factors remain unknown. An important finding is that a short-duration trigger with low pH can significantly enhance virus transduction efficiency, but the mechanism is poorly understood. Herein, we performed a detailed comparative study on entry mechanisms of the prototypical baculovirus *Autographa californica* multiple nucleopolyhedrovirus (AcMNPV) into insect and mammalian cells. The results showed that AcMNPV could be internalized into mammalian cells efficiently, but fusion in early endosomes (EEs) appeared to be the major obstacle. Measurement of endosomal pH suggested that virus fusion might be restricted under relatively high-pH conditions in mammalian cells. Interestingly, mutations of the major viral fusion protein GP64 that conferred decreased fusogenicity did not affect virus infection of insect cells, whereas virus transduction into mammalian cells was severely impaired, suggesting a more stringent dependence on GP64 fusogenicity for AcMNPV entry into mammalian cells than into insect cells. An increase in the fusogenicity of GP64 mutants resulting from low pH triggered the rescue of fusion-deficient recombinant virus transduction efficiency. Based on the above-described findings, the pH of EEs was specifically reduced with a Na⁺/K⁺-ATPase inhibitor, and the AcMNPV transduction of many mammalian cells indeed became highly efficient. This study not only revealed the roadblocks to mammalian cell entry of baculovirus but also provides a new strategy for improving baculovirus-based gene delivery and therapy.

IMPORTANCE Baculoviruses can transduce a wide variety of mammalian cells but do so with low efficiency, which greatly limits their practical application as potential gene delivery vectors. So far, the understanding of baculovirus entry into mammalian cells is obscure, and the limiting stages and factors are unclear. In this study, by comparatively analyzing the mechanisms of baculovirus entry into mammalian and insect cells, virus fusion during the early stage of endocytosis was revealed as the major obstacle for efficient baculovirus transduction into mammalian cells. A higher fusogenicity of the major viral fusion protein GP64 was found to be required for virus entry into mammalian cells than for entry into insect cells. Interestingly, by decreasing the pH of early endosomes with a specific agent, virus transduction of a wide range of mammalian cells was greatly enhanced. This study uncovers the roadblocks to mammalian cell entry of baculoviruses and presents mechanisms to overcome the roadblocks.

KEYWORDS baculovirus, early endosome, entry, fusion, gene delivery, mammalian cells, transduction

Citation Hu L, Li Y, Ning Y-J, Deng F, Vlak JM, Hu Z, Wang H, Wang M. 2019. The major hurdle for effective baculovirus transduction into mammalian cells is passing early endosomes. *J Virol* 93:e00709-19. <https://doi.org/10.1128/JVI.00709-19>.

Editor Joanna L. Shisler, University of Illinois at Urbana Champaign

Copyright © 2019 American Society for Microbiology. All Rights Reserved.

Address correspondence to Hualin Wang, h.wang@wh.iiov.cn, or Manli Wang, wangml@wh.iiov.cn.

Received 29 April 2019

Accepted 7 May 2019

Accepted manuscript posted online 15 May 2019

Published 17 July 2019

Baculoviruses are a diverse family of enveloped large DNA viruses that cause systemic infection in their host insects. Although they infect insects in nature, baculoviruses can transduce and deliver foreign genes of large sizes into a wide range of mammalian cells (including human cells) without replicating or integrating genomically. Thus, baculoviruses, especially the prototypical baculovirus *Autographa californica* multiple nucleopolyhedrovirus (AcMNPV), have been considered an ideal vector for gene delivery and therapy in the past decades (1). However, AcMNPV entry into many mammalian cells exhibits low efficiency, which greatly limits the application of AcMNPV as a practical gene delivery and gene therapy vector (2).

AcMNPV is generally believed to infect insect cells via clathrin-mediated endocytosis, followed by low-pH-triggered fusion of the viral envelope with the endosomal membrane to release nucleocapsids into the cytosol (3). The released nucleocapsids are then transported into the cell nucleus via actin polymerization (4). Similar to the mechanism for insect cells, AcMNPV enters mammalian cells mainly through clathrin- and dynamin-dependent endocytosis (5–7). It has also been reported that AcMNPV transduces nonphagocytic human cells through a clathrin-independent pathway and hepatoma cells through both endocytosis and macropinocytosis (7, 8).

The major envelope fusion protein GP64 of AcMNPV plays an essential role in mediating virus-receptor binding, internalization, and membrane fusion during virus entry into both mammalian and insect cells (9, 10). GP64 is a class III viral fusion protein that shares certain typical features with the G protein of rhabdoviruses, the gB protein of herpesviruses, and the glycoprotein (GP75) of thogotoviruses (11). The fusogenicity of GP64 is low pH dependent, and fusion of viral envelopes with the endosomal membrane is triggered in the acidic endosomal lumen. A pH lower than 5.5 is required for activation of GP64 to mediate efficient cell-to-cell fusion and virus-liposome fusion, although weak fusion was observed at pHs of 5.5 to 6.5 for the latter (12, 13). Interestingly, GP64 occurs only in one lineage of *Baculoviridae* (group I *Alphabaculovirus*). Thus, phylogenetic analysis suggested that GP64 may have been captured from a tick-borne thogotovirus by an ancestral group I alphabaculovirus during coevolution with their hosts, rendering the virus with a wider host range, higher infectivity, and accidentally, even the ability to enter mammalian cells (11, 14).

Many efforts have been made to improve the transduction efficiency of AcMNPV. One method is to display cell affinity proteins or peptides on the viral envelope by fusing them with GP64, the major envelope glycoprotein of AcMNPV (15–17). Another approach is to incorporate fusion proteins of other viruses, such as vesicular stomatitis virus (VSV) G protein (18) and influenza virus neuraminidase (19). Besides genetic modification, an important finding is that a short-duration trigger with low pH after virus binding to cells can significantly improve the transduction efficiency of AcMNPV, by more than 10-fold in various mammalian cells (6). In this case, the viral envelope fuses with the plasma membrane and nucleocapsids are directly released into the cytosol, avoiding the normal endocytosis pathway by utilizing the direct-fusion pathway. However, this does not increase the level of virus infection in insect cells.

It remains unclear why AcMNPV transduction of mammalian cells is inefficient and, mechanistically, how a low-pH trigger can drastically improve the entry efficiency of AcMNPV into mammalian cells but not into its insect host cells. To address these questions, we compared the entry mechanisms of AcMNPV into insect and mammalian cells in detail by employing a fluorescence-dequenching assay combined with multicolor-labeling technology and entry inhibitors. Our results showed that inefficient virus-endosome fusion in early endosomes (EEs) poses a major barrier to efficient AcMNPV entry into mammalian cells. By decreasing EE pH, the transduction efficiency of AcMNPV in mammalian cells was greatly improved. Thus, this study sheds light on the baculovirus entry mechanisms into mammalian cells in comparison with insect cells and may contribute to the further improvement of baculoviral gene therapy vectors.

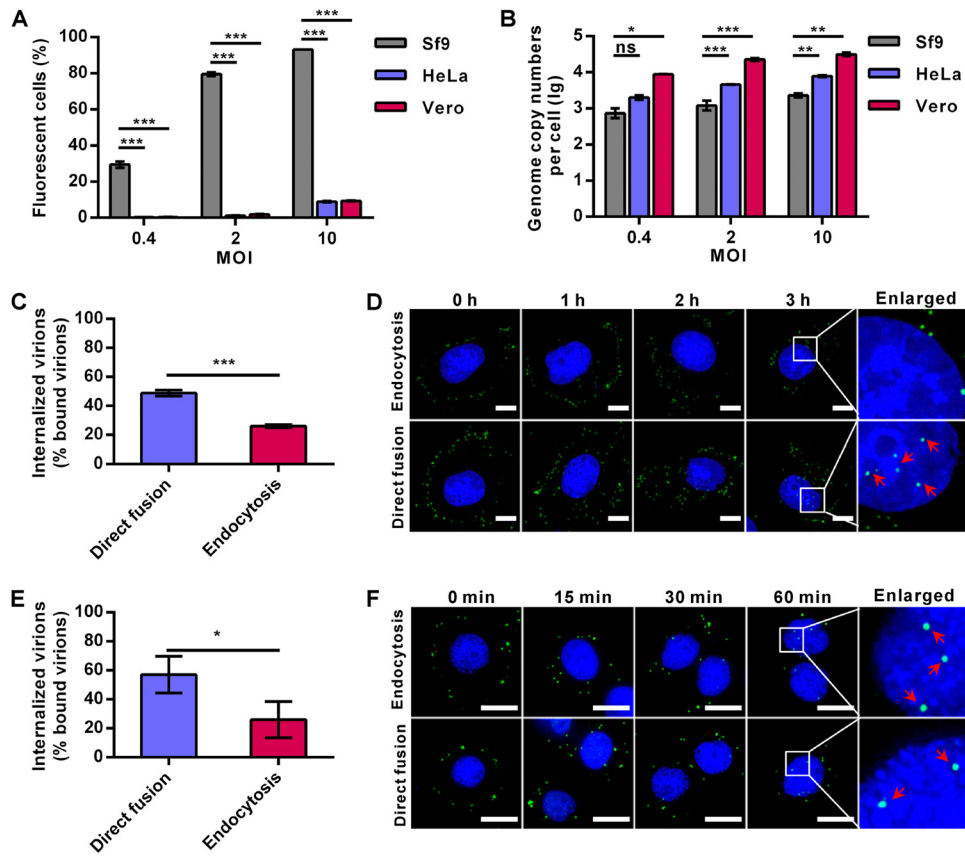


FIG 1 AcMNPV binds to and enters mammalian cells efficiently but is transported to the nucleus inefficiently. (A) AcMNPV infection/transduction of different cells. Sf9, HeLa, and Vero cells were infected/transduced with Ac-BPegfp at the indicated MOIs, after which the EGFP-positive cells were analyzed by FCM at 16 h p.i. (Sf9) or 24 h p.t. (HeLa and Vero cells). (B) AcMNPV binding to different cells. Sf9, HeLa, and Vero cells were incubated with Ac-BPegfp at 4°C to allow virus binding, and the quantities of cell-bound virions were measured by qPCR. (C and E) Virus internalization in HeLa (C) and Sf9 (E) cells. Cells were incubated with Ac-BPegfp at 4°C for 1 h to allow synchronous virus binding and then cultured for another 1 h before being collected for qPCR to quantify the amounts of internalized virions. (D and F) Virus entry into HeLa (D) and Sf9 (F) cells was detected by immunofluorescence microscopy. Cells were transduced/infected with Ac-BPegfp via the endocytosis or direct-fusion pathway and fixed at the indicated time points. Virions were detected by anti-VP39 antibody (green), and cell nuclei were stained with Hoechst 33258 (blue). Red arrows indicate the virions in cell nuclei. Bars, 10 μ m. For panels A to C and E, the results are mean values \pm standard deviations (SD) ($n = 3$ experimental replicates). Statistical analysis was performed using the unpaired *t* test: *, $P < 0.05$; **, $P < 0.01$; ***, $P < 0.001$.

RESULTS

AcMNPV enters mammalian cells efficiently, but further nucleocapsid transport into the nucleus is blocked.

AcMNPV can enter many mammalian cells, but only with low efficiency. As expected, the transduction rates of Ac-BPegfp (a recombinant virus with an *egfp* reporter gene, encoding enhanced green fluorescent protein [EGFP], under the control of promoters P_{Op166} and P_{CMV} , which can be expressed in both insect and mammalian cells) in both HeLa and Vero cells were only $\sim 9\%$ at a multiplicity of infection (MOI) of 10 50% tissue culture infective dose (TCID₅₀) units/cell, whereas the infection rates in *Spodoptera frugiperda* 9 (Sf9) cells reached $\sim 29\%$, $\sim 79\%$, and $\sim 93\%$ at MOIs of 0.4, 2, and 10 TCID₅₀ units/cell, respectively (Fig. 1A). However, the amounts of virions bound to HeLa cells were of comparable (MOI of 0.4 TCID₅₀ units/cell) or significantly higher (~ 2.7 - and ~ 3.9 -fold increases at MOIs of 2 and 10 TCID₅₀ units/cell, respectively) levels than those bound to Sf9 cells. For Vero cells, the numbers of bound virions were even higher (~ 12 - to ~ 19 -fold) than those of Sf9 cells at the same MOIs (Fig. 1B). These results indicate that AcMNPV can bind to mammalian cells with an equal or even higher affinity than to insect cells.

Generally, after binding to the plasma membrane, virions are endocytosed into the cytoplasm and nucleocapsids are released from endosomes and eventually transported to the nucleus. After virus binding, a short-time low-pH treatment could trigger AcMNPV fusion at the plasma membrane and release nucleocapsids directly into the cytosol (which is called the direct-fusion pathway) (6). Thus, the internalization of AcMNPV in HeLa cells and Sf9 cells via the endocytosis pathway was compared with that via the direct-fusion pathway, using the inhibitor bafilomycin A1 (BFA1) to block virus endocytosis (6). Cells were incubated with Ac-BPegfp at 4°C to allow virus binding, and the cell-bound virions were quantified by quantitative PCR (qPCR). To measure internalized virions, virus-bound cells were kept at neutral pH (7.3) or low pH (4.8) in phosphate-buffered saline (PBS) for a short time to allow virus entry through the endocytosis or direct-fusion pathway, respectively. After culturing for 1 h, the residual cell-bound virions were removed by trypsin digestion and the amount of internalized virions was measured by qPCR. Quantification of the results showed that ~49% and ~26% of bound virions were internalized into HeLa cells via the direct-fusion and endocytosis pathways, respectively, at 1 h posttransduction (p.t.) (Fig. 1C). However, immunofluorescence microscopy detected virus particles in the nuclei of HeLa cells transduced via the direct-fusion pathway but not via the endocytosis pathway up to 3 h p.t. (Fig. 1D). Similar to the results for HeLa cells, internalized virus particles in Sf9 cells were ~57% and ~26% of the cell-bound virions for the direct-fusion and endocytosis pathways, respectively, at 60 min postinfection (p.i.) (Fig. 1E). However, in contrast to the results for HeLa cells, virus particles were observed in the nuclei of Sf9 cells at 60 min p.i. via both pathways (Fig. 1F). These results suggest that internalization of AcMNPV into mammalian cells via endocytosis is as efficient as internalization into insect cells. However, virus release from endosomes and/or further nucleocapsid entry into the nucleus of mammalian cells was severely impaired.

Inefficient virus-endosome fusion restricts the entry of AcMNPV into mammalian cells. Virus-endosome membrane fusion is an essential step for enveloped viruses to escape from endosomes. To visualize virus fusion, AcMNPV was labeled with 1,1'-dioctadecyl-3,3,3',3'-tetramethylindodicarbocyanine (DiD). DiD is a lipophilic dye that displays fluorescence self-quenching at high concentrations and dequenches with a significant increase in fluorescence intensity when diluted as a result of viral envelope and endosomal membrane fusion (20). This was seen when the DiD-labeled virus (Ac-DiD) was triggered to fuse with the plasma membrane of HeLa or Sf9 cells by low pH (pH 4.8) and fluorescence intensity around the cell surface increased significantly (data not shown). Virus titration showed that DiD labeling did not impair the infectivity of AcMNPV (data not shown). When Ac-DiD was used to transduce HeLa cells via the normal endocytosis pathway, a few bright DiD fluorescence dots appeared in the cytoplasm at 20 min p.t., which then gradually increased in number (Fig. 2A, top). In Sf9 cells, bright DiD fluorescence dots occurred as early as 10 min p.i. and the overall fluorescence intensity was much higher than that in HeLa cells (Fig. 2A, bottom). We then measured the DiD fluorescence intensities of single virus particles ($n > 300$) every 10 min. The threshold for defining DiD dequenching (membrane fusion) was set as 1.5-fold of the mean DiD fluorescence intensity at 0 min p.t. (Fig. 2B and C). In HeLa cells, very little virus fusion occurred at 20 min p.t., less than 5% of Ac-DiD was fused at 30 min p.t. and only ~14% of the total number of virions was fused at 60 min p.i. (Fig. 2B and D). Meanwhile, in Sf9 cells, dequenched DiD reached approximately 30% as early as 10 min p.i. and increased to 50% at 40 min p.i. (Fig. 2C and D). These results show that AcMNPV fusion within its native host cells is much more rapid and efficient than in mammalian cells. This strongly suggests that inefficient virus fusion is the rate-limiting step during AcMNPV transduction of mammalian cells.

To accurately visualize the fusion site of AcMNPV during endocytosis, cells were transfected with plasmids coexpressing Rab5-fused EGFP (Rab5^{EGFP}) and Rab7-fused mCherry (Rab7^{mCherry}), markers for EEs and late endosomes (LEs), respectively (Fig. 2E). In HeLa cells, at the initial time point of virus fusion (20 min p.t.), ~35%, ~50%, and ~8% of dequenched DiD colocalized with Rab5- (EE), Rab5-/Rab7- (maturing endosome

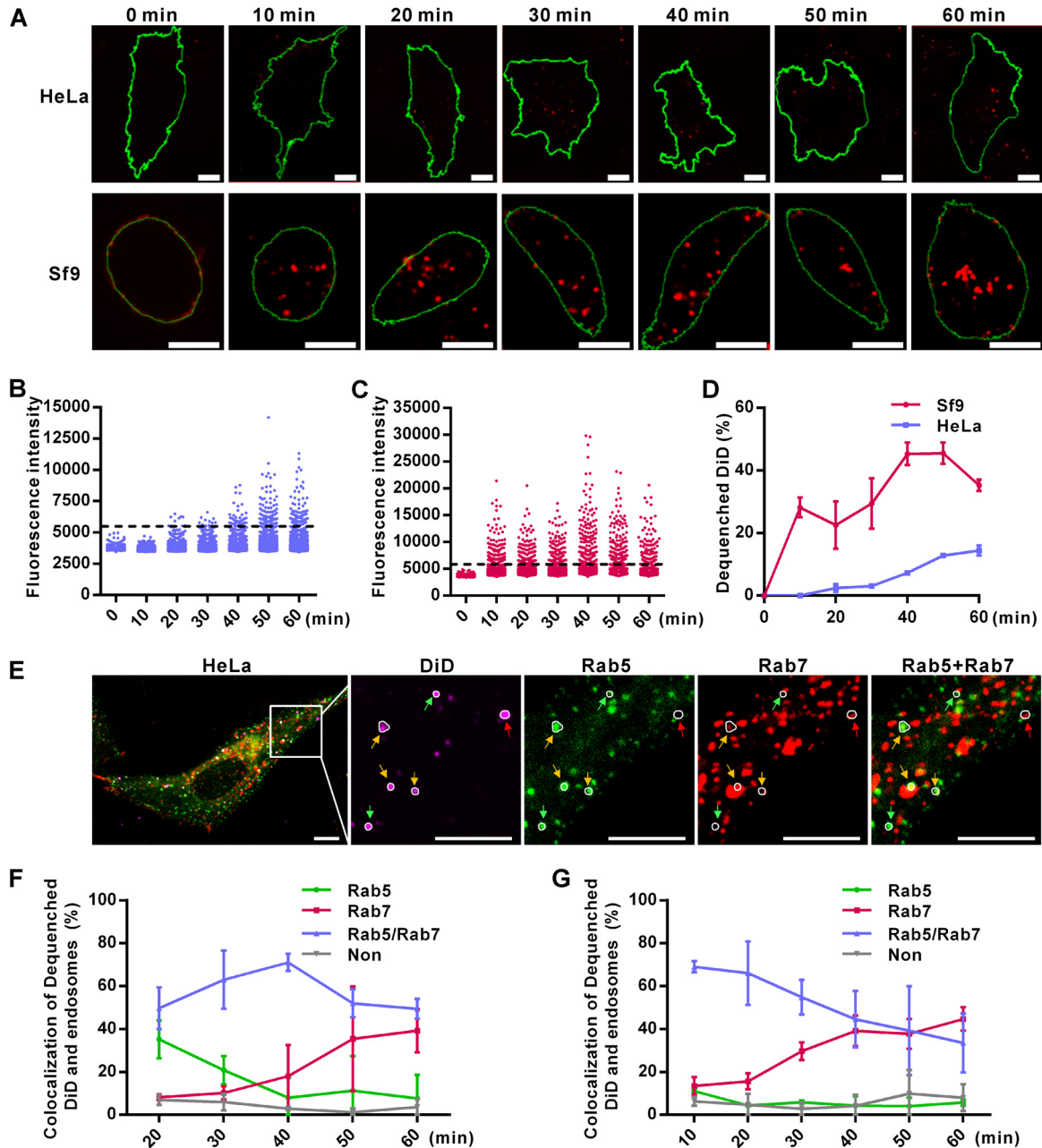


FIG 2 Inefficient virus-endosome fusion restricts the entry of AcMNPV into mammalian cells. (A) Detection of virus-endosome fusion by DiD-dequenching methodology. HeLa and Sf9 cells were incubated with DiD-labeled virus (Ac-DiD; MOI of 200 TCID₅₀ units/cell) at 4°C to allow virus binding, cultured at 37°C (HeLa cells) or 27°C (Sf9 cells) for indicated times, and imaged via fluorescence microscopy. Red dots indicate DiD fluorescence, and green lines outline the cells. Bars, 10 μm. (B and C) Changes in DiD fluorescence intensities in HeLa (B) and Sf9 (C) cells. Five randomly selected microscope fields from the experiment whose results are shown in panel A were analyzed at each time point. Dashed lines indicate the thresholds for defining dequenched DiD. (D) Percentages of dequenched DiD. Images from the experiment whose results are shown in panel A were analyzed for DiD intensity, and the percentages of dequenched DiD were calculated. The results are mean values ± SD (*n* = 2 independent experiments). (E) Colocalization of dequenched DiD and endosomes in HeLa cells at 20 min p.t. Cells transfected with plasmids expressing Rab5^{EGFP} and Rab7^{mCherry} were transduced by Ac-DiD (MOI of 200 TCID₅₀ units/cell) and imaged. Dequenched DiD loci were determined and are indicated by white circles. Dequenched DiD colocalized with Rab5-, Rab7-, or Rab5+Rab7-marked endosomes is indicated by green, red, and yellow arrows, respectively. (F and G) Statistics of colocalization of dequenched DiD and endosomes in HeLa (F) and Sf9 (G) cells analyzed as described for panel E. “Non” represents dequenched DiD that was not located in Rab5- or Rab7-marked endosomes. More than 20 randomly selected cells were analyzed at each time point. The results are mean values ± SD (*n* = 2 independent experiments). Bars, 10 μm.

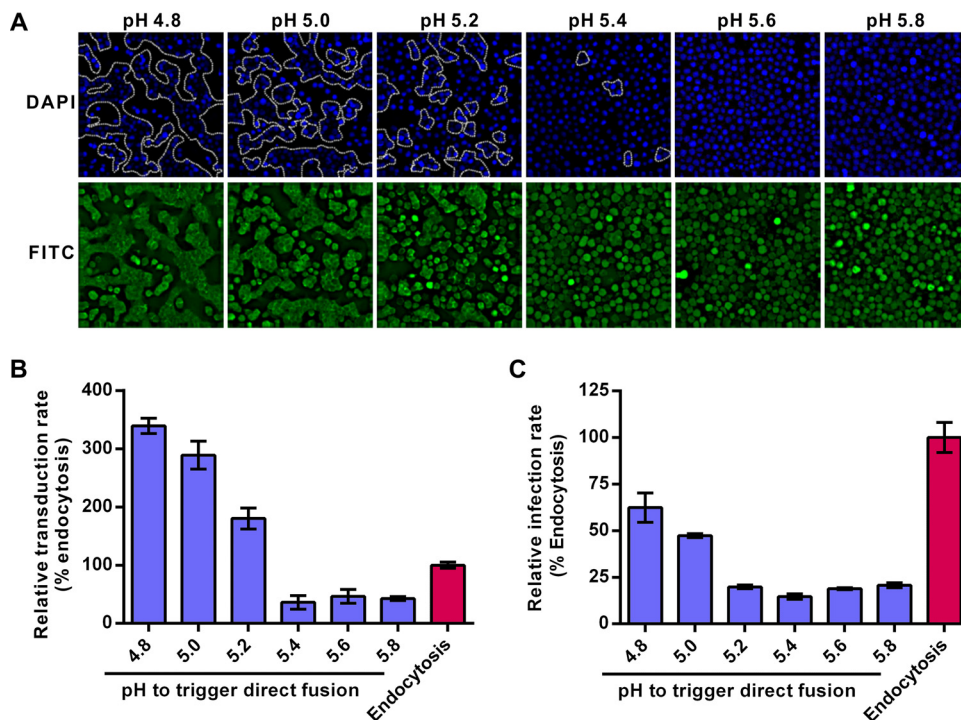


FIG 3 A pH of ≤ 5.4 is essential for activating the GP64 fusogenicity needed for AcMNPV entry. (A) Fusogenicity of GP64 at different pHs. Sf9 cells were infected with Ac-BPegfp (MOI of 5 TCID₅₀ units/cell) and treated with PBS (pH as indicated) to trigger syncytium formation. Cell nuclei were counterstained (DAPI [4',6-diamidino-2-phenylindole]; blue), and the syncytia are outlined (white dotted lines). The FITC channel (green) shows EGFP expression of infected cells. (B and C) HEK 293 cells (B) and Sf9 cells (C) transduced/infected with AcMNPV via the direct-fusion pathway as triggered by different pH values. Cells were incubated with Ac-BPegfp (MOI of 10 TCID₅₀ units/cell for HEK 293 cells or MOI of 0.2 TCID₅₀ units/cell for Sf9 cells) and treated with PBS (pH as indicated) to trigger the direct-fusion pathway. BFA1 (20 nM) was used to block the endocytosis pathway. The percentages of transduced/infected HEK 293 and Sf9 cells were quantified by FCM at 24 h p.t. (HEK 293 cells) or 16 h p.i. (Sf9 cells). The results were normalized to those of the endocytosis pathway. All results are mean values \pm SD ($n = 3$ experimental replicates).

[ME]), and Rab7 (LE)-positive vesicles, respectively (Fig. 2F). In Sf9 cells, the rates of colocalization of dequenched DiD with EEs, MEs, and LEs were $\sim 10\%$, $\sim 70\%$, and $\sim 13\%$, respectively, at 10 min p.i. (Fig. 2G). As infection progressed, more dequenched DiD was found colocalized with LEs in both insect and mammalian cells (Fig. 2F and G, red lines), which could be due to fusion occurring in LEs or the maturation of virus-fused EEs to LEs. However, during the entry stage, a smaller portion of virions fused with EEs in Sf9 cells than in HeLa cells (Fig. 2F and G). These results imply that AcMNPV fusion is likely to occur at a relatively earlier stage of endocytosis in HeLa cells than in Sf9 cells.

pH 5.4 or lower is required to enhance GP64 fusogenicity for efficient AcMNPV entry. The above-described results indicate that endocytic entry of AcMNPV is restricted during viral fusion. In the direct-fusion pathway, low-pH triggering of cell-bound virions activates the fusogenicity of GP64, which may lead virions to efficiently fuse with the plasma membrane and bypass the endosome barrier (6). Therefore, the entry efficiency of AcMNPV via the direct-fusion pathway is expected to be closely linked to GP64 fusogenicity. To test this hypothesis, the fusogenicity of GP64 was first examined at different pHs by the syncytium formation assay in Sf9 cells. The results showed that with a decrease in pH, the number and size of syncytia increased. When the pH was higher than 5.4, no obvious multinuclear cells were observed (Fig. 3A), which agrees with earlier reports that pHs lower than 5.5 are required for GP64-mediated fusion (12, 21). Our results confirmed that the fusogenicity of GP64 is low pH dependent and is efficiently activated at pHs of ≤ 5.4 .

We then analyzed how AcMNPV entry via the direct-fusion pathway was affected when virion-bound cells were exposed to different external pH conditions. In mammalian HEK 293 cells, which are more susceptible to AcMNPV transduction than are HeLa cells, treatment with pHs of ≥ 5.4 failed to trigger virus entry and resulted in transduction rates lower than that of the endocytosis pathway (Fig. 3B). Treatment of cells with pHs 5.2, 5.0, and 4.8 improved the transduction rate by 1.8-, 3.0-, and 3.5-fold, respectively, compared to that of the endocytosis pathway (Fig. 3B). For Sf9 cells, although treatment with pH 4.8 showed the highest infection activity in the direct-fusion pathway, the infection rate was only 60% of that of the endocytosis pathway (Fig. 3C). These results suggest that AcMNPV entry via the low-pH-triggered direct-fusion pathway is not as efficient as the endocytic pathway in insect cells, but the situation is the opposite in mammalian cells. Acidity of pH ≤ 5.4 may be required to activate GP64 to mediate efficient fusion between the viral envelope and cell plasma membranes of both mammalian and insect cells and is probably also applicable for virus–endosomal-membrane fusion.

Higher GP64 fusogenicity is required to mediate AcMNPV entry into mammalian cells than into insect cells. To find out the possible relationship between GP64 fusogenicity and virus entry efficiency, we attempted to construct GP64 mutants with altered fusion activities. Based on the amino acid conservation and crystal structure of GP64, two conserved acidic aspartic acids, D295 and D301, were replaced with glutamic acid individually (D295E or D301E) or in tandem (D295E/D301E). Both D295 and D301 are localized in random coils in the predicted prefusion structure of GP64, while D301 (but not D295) shifts into the central alpha-helix in the postfusion structure (Fig. 4A). Therefore, the D301E mutant was expected to have a more profound influence than the D295E mutant on the fusogenicity of GP64. These GP64 mutants were inserted into a previously constructed *gp64*-null bacmid containing a reporter *egfp* gene under the control of promoters P_{Op166} and P_{CMV} . Sf9 cells were transfected with the recombinant bacmids, and infectious recombinant viruses were obtained (Fig. 4B). The total cellular expression and cell surface display levels of the mutated GP64 were measured, showing no significant difference from those of the wild-type (WT) GP64 (Fig. 4C and D).

The fusion activities of GP64 mutants were then examined by a syncytium formation assay in Sf9 cells. As expected, the D295E mutant showed slightly reduced membrane fusogenicity that was 88% of the WT GP64 level, while the D301E mutant and the double-site D295E/D301E mutant showed dramatic reductions in fusion ability, at only 7% and 10% of WT GP64 fusogenicity, respectively (Fig. 5A). One-step growth curve analysis of Sf9 cells showed that the levels of infectious virus production of the D301E and D295E/D301E mutants were similar to that of the WT virus, whereas the D295E mutant had a small but statistically significant increase in virus titer at 72 h p.i. ($P < 0.05$) (Fig. 5B). These results suggest that GP64 mutants with decreased fusogenicity did not have impaired virus infection of insect cells.

Interestingly, the virus transduction efficiencies for HEK 293 cells showed a close correlation with the fusogenicities of GP64 mutants (Fig. 5C to E). The transduction rate of the D295E mutant (at $\sim 88\%$ of WT GP64 fusogenicity) decreased to $\sim 80\%$ of the WT virus level (Fig. 5C and D). The D301E and D295E/D301E mutants—with very weak fusogenicities—showed severely decreased transduction efficiencies at only $\sim 9\%$ and $\sim 30\%$ of the WT level, respectively. Linear-regression analysis indicated that transduction efficiency and membrane fusogenicity were closely correlated ($R^2 = 0.96$, $P < 0.05$; Fig. 5E). These results suggest that the fusion activity of GP64 has a more profound impact on AcMNPV entry into mammalian cells than into insect cells.

Similar to that of the WT GP64, the fusogenicity of GP64 mutants increased when pH decreased (data not shown). Although the transduction rate of D301E mutants via endocytosis in HEK 293 cells was only $\sim 9\%$ of the WT virus rate, the entry of the D301E mutant was significantly enhanced after pH 5.4 treatment and increased to up to $\sim 80\%$ of the WT virus rate at pHs of ≤ 5.2 (Fig. 5F). For the other mutants, reduced transduction efficiency was also enhanced to different extents after low-pH treatment (pH 4.8) (Fig. 5G). These results suggest that low-pH treatment can significantly rescue entry of

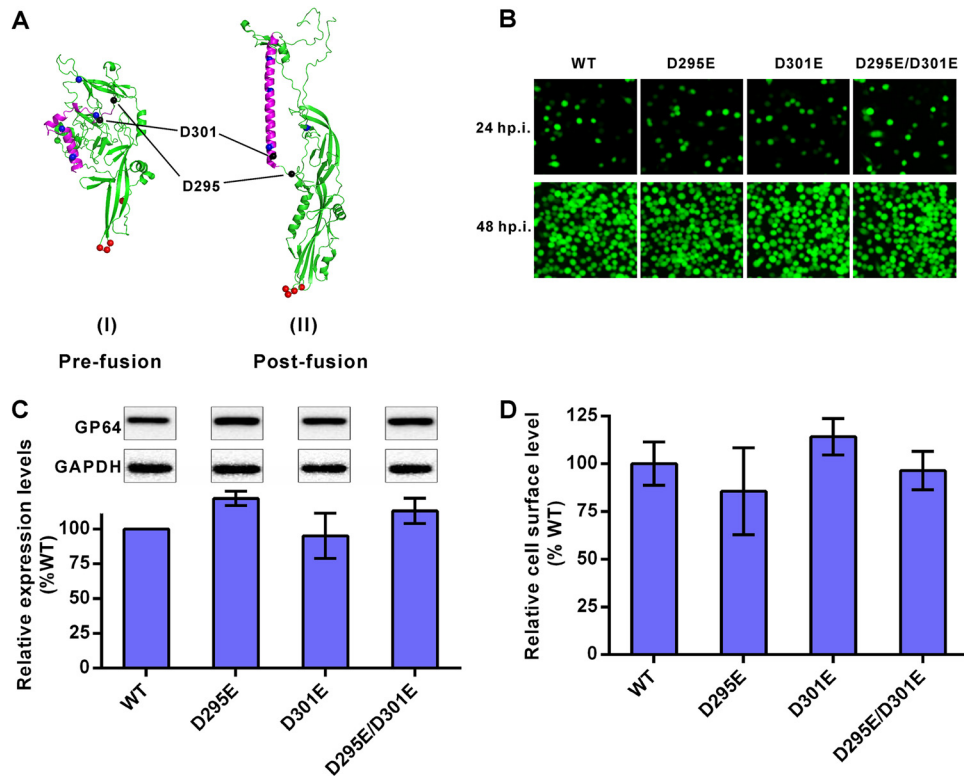


FIG 4 Construction of recombinant AcMNPV containing mutated GP64. (A) Three-dimensional structures of GP64. Predominant coiled-coil (purple), pH-sensitive histidine (blue dots), fusion loop (red dots), and D295 and D301 (black dots) are indicated. The pre-fusion structure is a predicted model, and the postfusion structure is based on GP64 data in the Protein Data Bank (PDB code [3DUZ](#)) (48). (B) Infection assay. Sf9 cells were infected by recombinant viruses at an MOI of 1 TCID₅₀ unit/cell and imaged at 24 and 48 h p.i. (C) Expression levels of mutated GP64. Sf9 cells were infected by recombinant viruses at an MOI of 5 TCID₅₀ units/cell and collected for Western blot analysis at 48 h p.i. Expression levels of GP64 were determined by dividing the values for GP64 by those for glyceraldehyde-3-phosphate dehydrogenase (GAPDH). The results were normalized to those of WT GP64. All results are mean values \pm SD ($n = 3$ independent experiments). (D) Analysis of cell surface-displayed mutated GP64. Sf9 cells were infected by recombinant viruses at an MOI of 5 TCID₅₀ units/cell for 48 h and fixed, and the amounts of GP64 protein on cell surfaces were measured via cell surface ELISA. The results were normalized to those of WT GP64. All results are mean values \pm SD ($n = 3$ experimental replicates). For the data shown in panels C and D, statistical analysis was performed using the unpaired *t* test, and no significant difference was found between the results for the mutants and the WT control ($P > 0.05$).

low-fusogenicity AcMNPV GP64 mutants into mammalian cells, probably via enhancing fusion activities of the mutants.

AcMNPV fusion occurs in higher-pH endosomes in mammalian cells than in insect cells. BFA1 is an inhibitor of vacuolar H⁺-ATPase, while NH₄Cl is a biologically weak base that accumulates in the endosome/lysosome. Treatment with BFA1 or NH₄Cl results in an increase in endosomal pH (22, 23). Both BFA1 (10 nM) and NH₄Cl (10 mM) inhibited Ac-BPegfp infection of Sf9 cells, reducing the infection rates from 100% of the rate in the untreated control to 0.8% and 12%, respectively (Fig. 6A), which is consistent with previous reports (6, 24). The inhibitory effect of BFA1 on virus transduction of HeLa cells occurred in a dose-dependent manner, as 10, 20, and 40 nM BFA1 reduced the transduction rates to 82%, 22%, and 2.0% of the rate in the control, respectively (Fig. 6B). However, in contrast to the results for insect cells, NH₄Cl did not inhibit virus transduction of HeLa cells even at concentrations as high as 40 mM (Fig. 6B). A similar effect was also observed when HEK 293 and HEK 293T cells were transduced with AcMNPV (data not shown). A recombinant VSV with an *egfp* marker gene (VSV-GFP) that enters cells through the endocytosis pathway and fuses with LEs (25) was used as a positive control. The results showed that both 10 nM BFA1 and 10 mM NH₄Cl inhibited VSV-GFP infection of HeLa cells, leading to reduced infectivities of 7% and 8% of the infectivity in the untreated control, respectively (Fig. 6C).

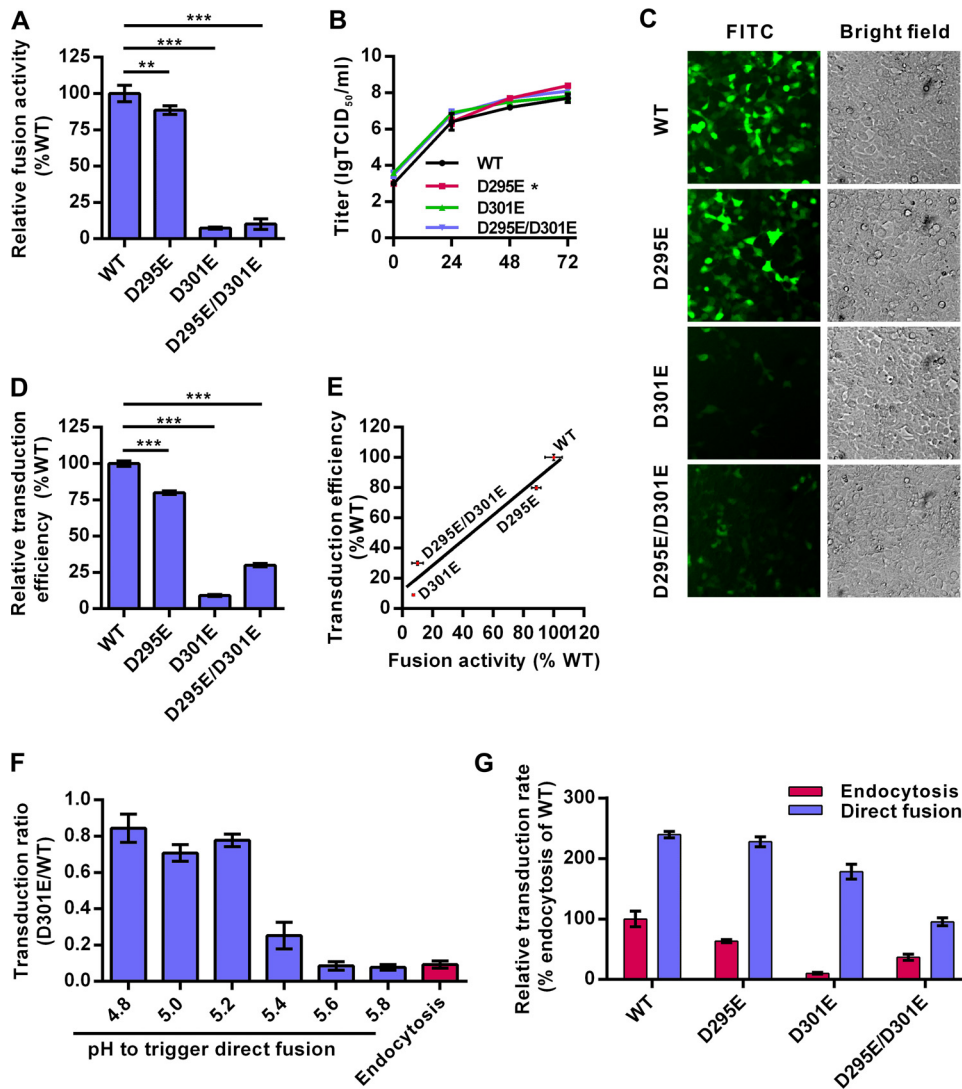


FIG 5 The fusogenicity of GP64 is strictly associated with the transduction efficiency in mammalian cells. (A) Fusogenicity of GP64 mutants. Sf9 cells were infected with recombinant AcMNPVs (MOI of 5 TCID₅₀ units/cell) for 48 h, and the syncytium formation assay was performed. Fusogenicity was determined by dividing the number of nuclei in syncytia by the total number of cells in a field. Data were normalized to those of WT virus. (B) One-step growth curves of the various recombinant viruses. (C) HEK 293 cells were transduced with recombinant viruses at an MOI of 10 TCID₅₀ units/cell and imaged for EGFP expression at 24 h p.t. (D) HEK 293 cells transduced with recombinant viruses as described in the legend to panel C were analyzed by FCM. Data were normalized to those of the WT virus. (E) Correlation of transduction efficiency and fusogenicity. Linear regression analysis was performed, and the trend line is displayed on the scatter plot, for which the function is $Y = 0.8345 \times X + 11.79$ ($R^2 = 0.96$). (F) The transduction of GP64 D301E mutation-containing virus was rescued by a low-pH trigger. Cells were incubated with D301E or WT virus at 4°C and treated with PBS (pH as indicated) to trigger the direct-fusion pathway. BFA1 (20 nM) was used to block the endocytosis pathway. The percentage of EGFP-positive cells transduced with D301E virus was divided by that of cells transduced with the WT virus at each pH. (G) Low-pH trigger increases the transduction of recombinant viruses. HEK 293 cells were transduced with recombinant viruses through the endocytosis or direct-fusion (triggered with pH 4.8) pathway as described above. The results were normalized to those of WT transduction through the endocytosis pathway. For panels A, B, D, F, and G, all results are mean values \pm SD ($n = 3$ experimental replicates). Statistical analysis was performed using the unpaired *t* test: *, $P < 0.05$; **, $P < 0.01$; ***, $P < 0.001$.

To further explore the mechanism underlying the distinct inhibitory effects of BFA1 and NH₄Cl, we first confirmed that both inhibitors did not impair the internalization and transportation of AcMNPV from EEs to LEs in mammalian and insect cells (data not shown). Then, the inhibitory effects of the two reagents on virus-endosome fusion were analyzed by DiD-dequenching experiments. In Sf9 cells, both BFA1 (20 nM) and NH₄Cl (20 mM) inhibited virus fusion (Fig. 6D). In HeLa cells, BFA1 reduced the amount of

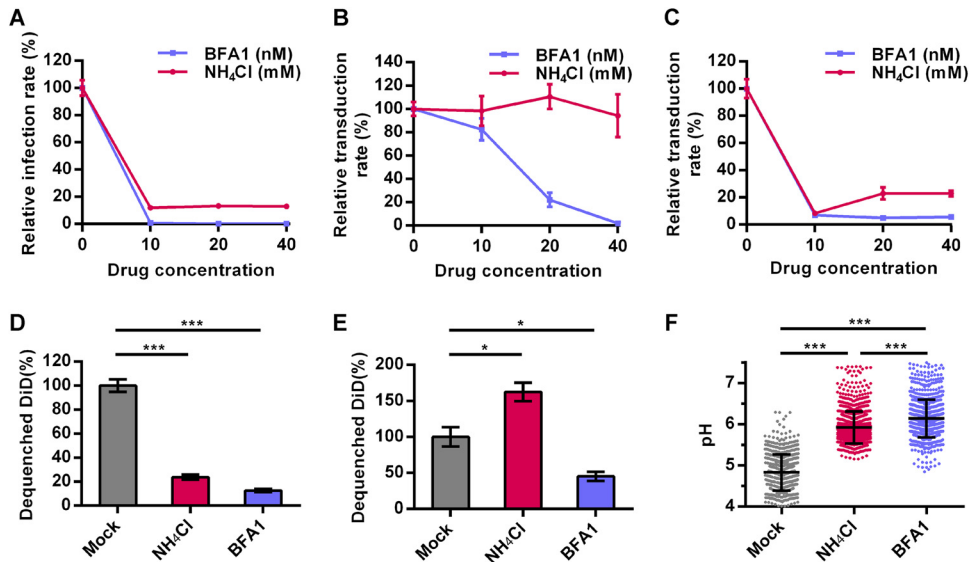


FIG 6 Two endosomal acidification inhibitors reveal the relatively high pH of the endosome where AcMNPV fuses in mammalian cells. (A to C) Effects of BFA1 and NH₄Cl on virus entry. Sf9 and HeLa cells were incubated with BFA1 or NH₄Cl at the indicated concentrations. Sf9 (A) and HeLa (B) cells were infected/transduced by Ac-BPegfp (MOI of 0.2 TCID₅₀ units/cell for Sf9 cells or MOI of 10 TCID₅₀ units/cell for HeLa cells). (C) HeLa cells were transduced by VSV-GFP. Cells were analyzed by FCM for EGFP expression at 24 h p.t. (HeLa cells) or 16 p.i. (Sf9 cells). (D and E) Effects of BFA1 and NH₄Cl on virus-endosome fusion. Sf9 (D) and HeLa (E) cells were incubated with 20 nM BFA1 or 20 mM NH₄Cl and infected/transduced by Ac-DiD (MOI of 200 TCID₅₀ units/cell). Cells were imaged at 60 min p.i./p.t. The fluorescence intensities of DiD were analyzed, and the percentages of dequenched DiD were calculated. (F) BFA1 and NH₄Cl increased endosomal pH. HeLa cells were incubated with 20 nM BFA1 or 20 mM NH₄Cl and stained with LSYB. Cells were imaged via fluorescence microscopy, and the pH of each endosome was calculated by ratiometric fluorescence measurement. Five randomly selected fields were analyzed per group. For panels A to E, the results were normalized to those of cells not treated with BFA1 and NH₄Cl. For panels A to C, all results are mean values \pm SD ($n = 3$ experimental replicates). For panels D and E, the results are mean values \pm SD ($n = 2$ independent experiments). Statistical analysis was performed using the unpaired *t* test: *, $P < 0.05$; **, $P < 0.01$; ***, $P < 0.001$.

dequenched DiD to 40% of the amount in the mock treatment group, whereas NH₄Cl increased virus fusion to 160% of that in the control (Fig. 6E). This may be the result of differences in elevated endosomal-pH levels following BFA1 and NH₄Cl treatment. To measure endosomal pH, HeLa cells were stained by LysoSensor yellow/blue DND-160 (LSYB), an acidotropic probe allowing pH calculation by ratiometric fluorescence microscopy (26). NH₄Cl (20 mM) and BFA1 (20 nM) significantly elevated the mean endosomal pHs, from 4.8 to 5.9 and 6.1, respectively (Fig. 6F). Moreover, the percentages of endosomes with pHs of >6.0 were 67% and 34% in BFA1- and NH₄Cl-treated cells, respectively (data not shown). These results show that BFA1 can increase endosomal pH to higher levels than can NH₄Cl. The fact that only BFA1, and not NH₄Cl, inhibited virus-endosome fusion implies that AcMNPV fusion in mammalian cells, which is not efficient, takes place in relatively high-pH ($\text{pH} \geq 5.9$) endocytic vesicles (generally EEs), which is beyond the neutralization range of NH₄Cl.

The entry block for AcMNPV in various mammalian cells can be removed by decreasing the pH of EEs. The above-described results indicate that AcMNPV entry into mammalian cells was halted within a relatively early stage during endocytosis when relatively high-pH conditions failed to efficiently activate GP64 fusogenicity for proper virus fusion and endosome escape. Therefore, we attempted to remove this entry restriction by decreasing the pH of endosomes. Ouabain, a small cardiac steroid molecule, was reported to specifically decrease the pH of EEs by inhibiting Na⁺/K⁺-ATPase and disturbing the interior positive membrane potential, thereby enhancing the activity of H⁺-ATPase (27, 28). Ouabain showed almost no cytotoxicity in all 11 cell lines we tested at a concentration of 0.8 μM , although ouabain at higher concentrations (4 μM and 20 μM) showed slight toxicity in HMC3, HEK 293, and Vero cells (the levels

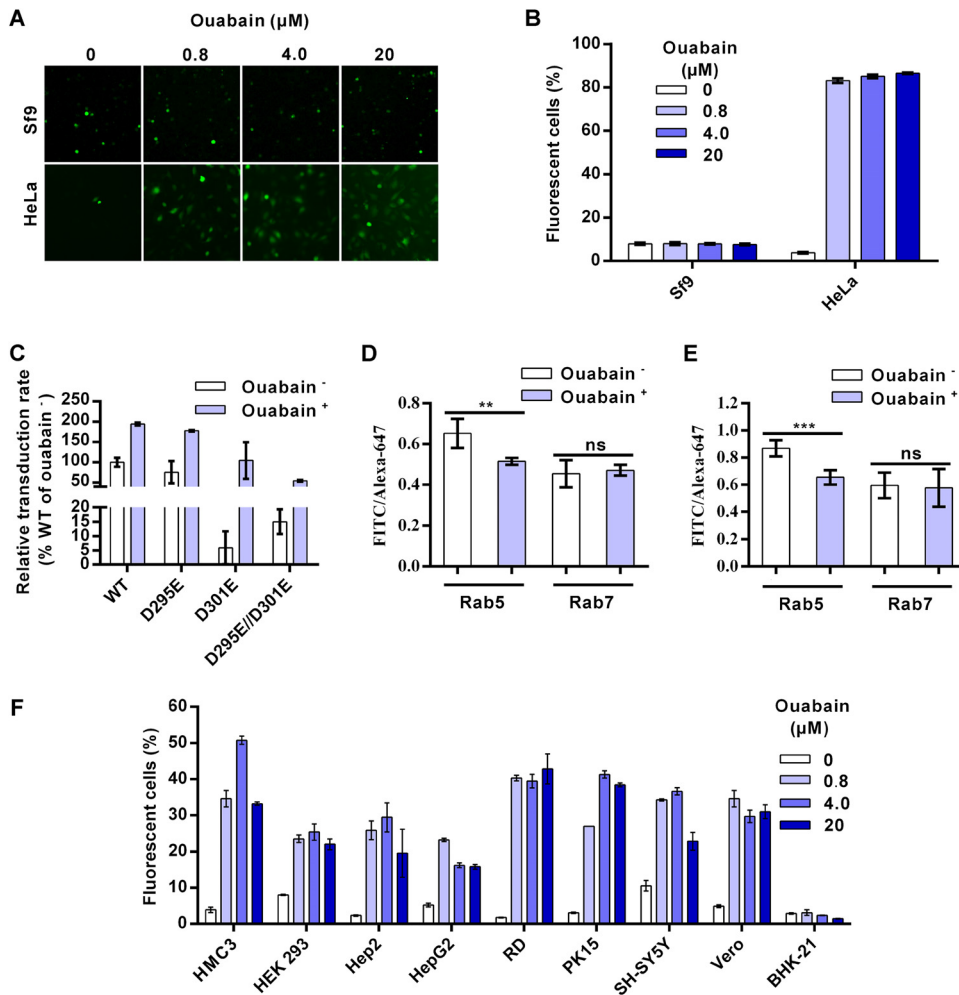


FIG 7 Ouabain increases AcMNPV transduction of mammalian cells by decreasing early endosome (EE) pH. (A) Sf9 and HeLa cells were treated with ouabain and infected/transduced by Ac-BPegfp at an MOI of 0.2 (Sf9 cells) or 5 (HeLa cells) TCID₅₀ units/cell. Cells were imaged at 16 h p.i. (Sf9 cells) or 24 h p.t. (HeLa cells). (B) FCM analysis of the effect of ouabain on virus transduction/infection as described in the legend to panel A. (C) Cells were treated with/without 0.8 μM ouabain, transduced by recombinant viruses containing mutated GP64 at an MOI of 5 TCID₅₀ units/cell, and analyzed by FCM at 24 h p.t. The results were normalized to those of WT virus treated without ouabain. (D and E) Ouabain decreased the EE pH. Sf9 (D) and HeLa (E) cells were transfected with plasmids expressing Rab5^{mCherry} or Rab7^{mCherry}. Cells were incubated with 0.8 μM ouabain and dextrans conjugated to FITC or Alexa Fluor 647. Cells were imaged via fluorescence microscopy, and then the relative endosomal pHs were calculated by ratiometric fluorescence measurements. The results are mean values ± SD (*n* = 4 independent experiments). (F) Effects of ouabain on virus transduction of different mammalian cells. Each cell line was treated with ouabain and transduced by Ac-BPegfp at an MOI of 5 TCID₅₀ units/cell, followed by analysis with FCM at 24 h p.t. For panels B, C, and F, all results are mean values ± SD (*n* = 3 experimental replicates). Statistical analysis was performed using the unpaired *t* test: *, *P* < 0.05; ***, *P* < 0.001; ns, not significant.

of cell viability were reduced to 76% to 86% of that of the mock treatment group) (data not shown). In insect Sf9 cells, there were no significant differences in AcMNPV infection rates when cells were treated or not with 0.8, 4, and 20 μM ouabain (Fig. 7A and B). In contrast, the virus transduction rates in HeLa cells increased from ~4% (control group) to ~83%, ~85%, and ~87% when cells were treated with 0.8, 4, and 20 μM ouabain, respectively (Fig. 7A and B). Ouabain also increased the transduction of recombinant viruses containing mutated GP64 in HEK 293 cells (Fig. 7C), as the transduction rates of the WT and the D295E, D301E, and D295E/D301E mutants increased by approximately 1.9-, 2.4-, 17.7-, and 3.6-fold, respectively, following a trend of improved virus transduction similar to that seen under low-pH conditions (Fig. 5G). We further confirmed the effect of ouabain on endosomal pH by ratiometric fluorescence measurements. Endosomes were labeled with Rab5^{mCherry} or Rab7^{mCherry} and dextrans conjugated

with pH-sensitive fluorescein isothiocyanate (FITC) and pH-insensitive Alexa Fluor 647 (Alexa-647). With decreasing pH levels, the fluorescence intensity of FITC decreases while that of Alexa-647 remains relatively stable (27). Thus, lower-intensity ratios of FITC/Alexa-647 represent lower pH values. Consistent with the previous report, we found that ouabain significantly decreased the pH of EEs but not LEs in both Sf9 and HeLa cells (Fig. 7D and E).

To find out whether ouabain can generally improve AcMNPV transduction of mammalian cells, eight mammalian cell lines apart from HeLa and HEK 293 cells were tested. For the six human cell lines (HCM3, Hep2, HepG2, RD, PK15, and SH-SY5Y) tested, virus transduction improved between ~3- and 25-fold compared with the levels in the control groups (Fig. 7F). Ouabain also increased the transduction rate by ~7-fold in the Vero monkey cell line. BHK-21 cells were an exception, as virus transduction in this hamster cell line did not improve. As a control, the entry efficiency of VSV-GFP, which fuses with LEs, did not improve in Hep2 cells but was slightly improved (<2-fold) in HeLa, RD, and Vero cells after ouabain treatment (data not shown). These results indicate that ouabain can remove the entry block for AcMNPV and improve the transduction of this versatile insect virus in various mammalian—especially human—cell lines.

DISCUSSION

AcMNPV can enter a wide range of mammalian cells via endocytosis but with low efficiency, which greatly limits its further development as a gene delivery and therapy vector (6, 29). A previous report showed that a low-pH trigger after virus binding to mammalian cells significantly enhances the entry efficiency of AcMNPV via direct fusion with the plasma membrane (6). This led us to speculate that endocytosis poses a barrier for efficient AcMNPV entry into mammalian cells. In the current study, through a detailed comparison of the entry process of AcMNPV into mammalian and insect cells, we demonstrated that AcMNPV can bind to and further internalize into mammalian cells (HeLa and Vero cells) efficiently (Fig. 1). However, virus-endosome fusion appears blocked during the early stage of endocytosis in mammalian cells compared with that of insect cells (Fig. 2). This is consistent with a previous report indicating that perturbation of the function of the EE by a dominant-negative Rab5 mutant, but not of the LE by that of Rab7, significantly reduced AcMNPV transduction in HeLa cells (30).

Virus fusion within acidic endosomes is balanced by the pH thresholds of viral fusion proteins and the actual endosomal pH. For example, the K58I mutation in hemagglutinin (HA) of avian influenza virus (H5N1) decreases the pH threshold of HA activation from 6.0 to 5.5 and reduces virus growth in A549 cells but not in MDCK cells, for which the mean endosomal pHs are 5.9 and 5.4, respectively (31). For WT GP64, the pH threshold of optimal fusogenicity is 5.4 (Fig. 3), while very weak fusogenicity was observed at pHs of 5.5 to 6.5 (13). Interestingly, the dramatically reduced transduction efficiency of the GP64 D301E mutant was effectively rescued by low-pH (<5.4) conditions (Fig. 5F). As summarized in Fig. 8A, the fusogenicities of both the D301E mutant and WT GP64 increased with decreasing pH. At pHs of ≥ 5.6 , the fusogenicity of WT GP64 was low and only small proportions of virions fused with the plasma membrane to release nucleocapsids. The GP64 D301E mutant showed even lower fusogenicity, and only ~8% of nucleocapsids were released compared with the amount for the WT virus, which is similar to the D301E mutant/WT ratio for transduction via the normal endocytosis pathway (Fig. 5D). When the pH dropped to 5.4, the fusogenicity of the D301E mutant was partially rescued, leading to an increase to ~25% of the WT AcMNPV transduction levels. At pHs of 4.8 to 5.2, the transduction rates of the D301E mutant increased to ~80% of the rate for WT AcMNPV, which is similar to the relative infection rates in insect cells. These findings indicate that the fusogenicity of this mutant at pHs of <5.4 can mediate virus fusion with the cellular membrane to levels comparable to that of the WT virus, suggesting that AcMNPV fusion occurs inefficiently during the early stage of endocytosis in mammalian cells, which have relatively higher pHs, and may occur with high efficiency in the more acidic LEs of insect cells.

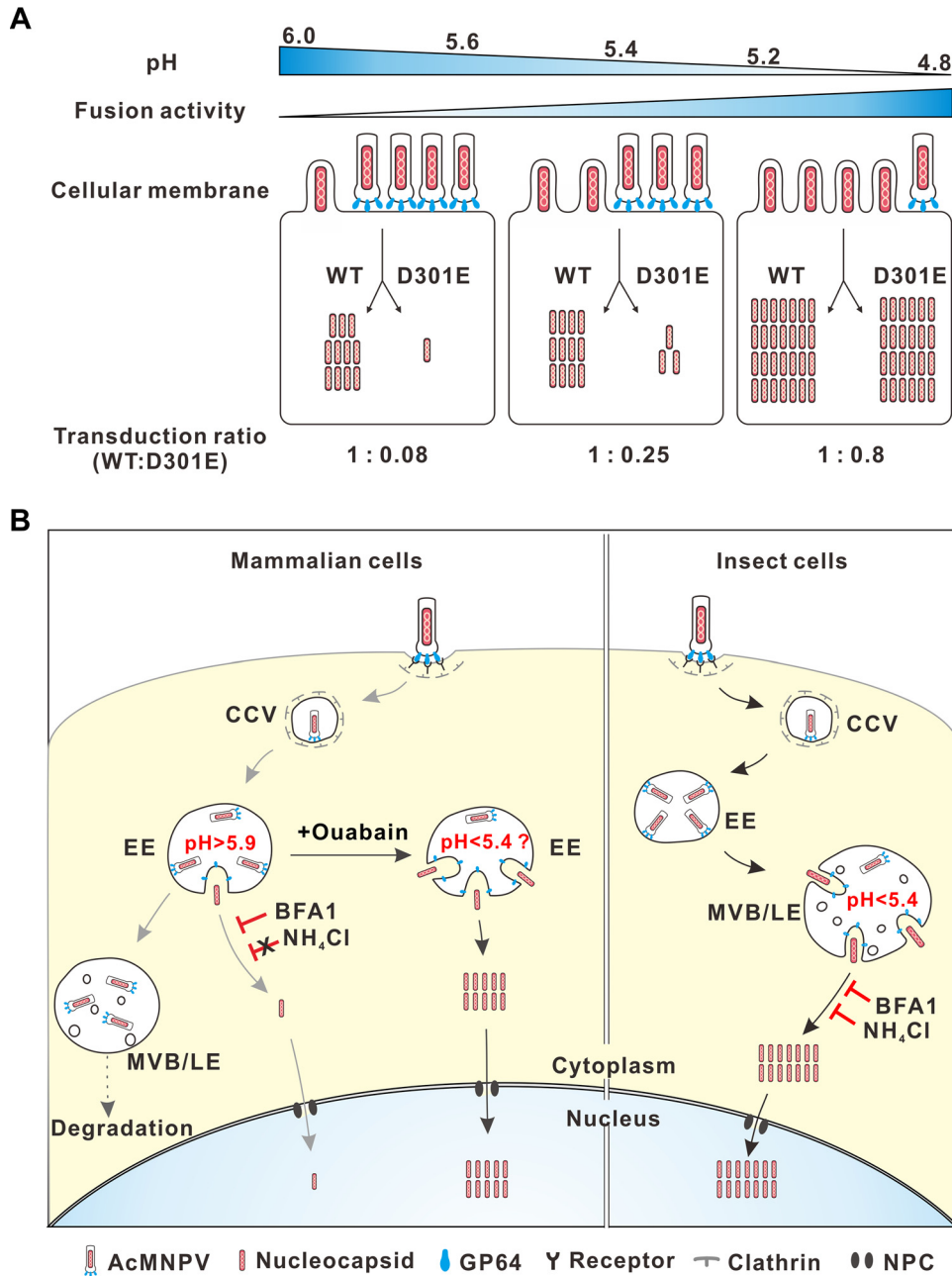


FIG 8 Schematic diagram illustrating the proposed mechanism of AcMNPV entry in mammalian and insect cells. (A) Entry of recombinant AcMNPV containing WT or mutated GP64 is regulated via pH. With decreased pH, especially at pHs lower than 5.4, the fusogenicities of the WT and D301E mutant GP64 increase, leading to increased virion fusion with the cellular membrane and increased nucleocapsid release. The fusogenicity of the D301E mutant increased relatively faster than that of the WT and was sufficient to mediate viral fusion at pHs of <5.4, rescuing the virus entry from 0.8% to 80% of WT levels. (B) Different entry mechanisms of AcMNPV in mammalian and insect cells. In mammalian cells, the virus is endocytosed into the clathrin-coated vesicles (CCVs) and transported to the EEs. Very few virions fuse here to release nucleocapsids into the cytoplasm. Most virions are restricted within the EEs and then transported to late endosomes (LEs) and, possibly, lysosomes for degradation. Ouabain can decrease the pH of the EEs, greatly enhancing viral fusion. In insect cells, the virus is also endocytosed and transported to the CCVs and EEs but, in contrast to the case for mammalian cells, fuses efficiently with the LEs. In both cell types, released nucleocapsids are transported to the nucleus through the nuclear pore complex (NPC).

BFA1 and NH₄Cl, two endosomal acidification inhibitors, blocked AcMNPV infection of insect cells and VSV infection of HeLa cells by inhibiting virus-endosome fusion (Fig. 6A and C). However, BFA1 inhibited AcMNPV transduction of HeLa, HEK 293, and

HEK 293T cells in a dose-dependent manner, whereas NH_4Cl could not, even at a concentration as high as 40 mM (Fig. 6B and data not shown). The results showed that NH_4Cl (20 mM) and BFA1 (20 nM) elevated the mean endosomal pHs to 5.9 and 6.1, respectively, which is in line with previous reports (26, 32). Indeed, to inhibit viral infection, the endosomal pH should be elevated higher than the pH threshold of the pertinent viral fusion protein to block viral fusion. For example, the infection of avian influenza virus strains Dk/Hk (H5N3) and Cw/Ky (H5N1), whose pHs of HA fusion activation are ~ 5.3 and ~ 5.6 , respectively, was markedly inhibited when the mean endosomal pHs were elevated from 5.01 to 5.54 and 5.95, respectively (33). These results indicate that virus-endosome fusion of AcMNPV may occur in the EEs of HeLa and HEK 293 cells at pHs of >5.9 .

Although the EE pHs of both insect Sf9 and mammalian HeLa cells decreased significantly after ouabain treatment, virus entry did not improve in Sf9 cells but increased up to ~ 20 -fold in HeLa cells (Fig. 7). These results further support the conclusion that AcMNPV fusion occurs efficiently in the LEs of insect cells but is blocked within the EEs of mammalian cells. Virus transduction in seven other human cell lines and one monkey cell line (Vero) was also substantially improved, by 3- to 25-fold, after ouabain treatment, suggesting a similar entry mechanism for AcMNPV in these cells. Therefore, ouabain may be further modified for better efficacy and less cytotoxicity and applied as a promising agent with broad activity for enhancing AcMNPV transduction of mammalian cells.

Based on our experiments and previous studies on AcMNPV entry, we propose a model that depicts the different entry mechanisms of AcMNPV into mammalian and insect cells (Fig. 8B). In mammalian cells, the cell-bound virions are internalized into the neutral clathrin-coated vesicles (CCVs) and then transferred to the slightly acidic EEs, where the weak fusogenicity of GP64 mediates restricted virus-endosome fusion that can be blocked by BFA1 but not by NH_4Cl . Nucleocapsids are then released and transported into the nucleus via the nuclear pore complex in an actin-dependent manner (5, 34). However, the majority of virions are still restricted in EEs, after which they are transported to LEs, losing their fusion ability for unknown reasons, and are finally degraded. With the aid of ouabain, EE pH is decreased to <5.4 , greatly increasing virus-endosome fusion and leading to effective transduction. In insect cells, AcMNPV virions are endocytosed into EEs and then transported into multivesicular bodies (MVBs)/LEs, where the lumen pH is ≤ 5.4 . The virions efficiently fuse with MVBs/LEs to release the majority of nucleocapsids for effective infection (3).

In conclusion, we showed that AcMNPV can bind to and internalize into mammalian cells, but inefficient virus-endosome fusion in EEs reduces the entry efficiency of AcMNPV. This block can be released by decreasing EE pH, which leads to significantly improved AcMNPV transduction in a wide variety of mammalian cells. It has been hypothesized that an ancestral group I alphabaculovirus obtained the prototypic GP64 (GP75) from a thogotovirus-like ancestor, which may have led to inheriting the tropism of thogotovirus in mammals (11). The pH threshold of GP75-mediated fusion is ~ 6.2 , which may aid efficient thogotovirus fusion with the EEs of vertebrate cells (35). However, GP64 may have adapted to insect host cells, shifting the pH threshold of fusion from 6.2 to 5.4 to avoid earlier conformational activation before virion transport to LEs. This possibly resulted in the poorly activated fusogenicity of GP64 in the EEs of mammalian cells during virus fusion. However, it is unclear why GP64-mediated fusion could not occur within more acidic LEs of mammalian cells. A possible explanation may be that the protein and/or lipid compositions of endosomes may vary greatly (36) and, hence, may determine the outcome of virus-endosome fusion, as reported in some viruses, including AcMNPV (13, 25, 37, 38).

Overall, our findings uncover why baculoviruses enter mammalian cells with low efficiency and provide a novel strategy for increasing GP64 fusogenicity by decreasing endosomal pH for further improvement of baculovirus-based gene delivery and therapy.

MATERIALS AND METHODS

Cell culture and viruses. BHK-21, HCM3, HEK 293, HEK 293T, HeLa, HepG2, RD, SH-SY5Y, and Vero cells were obtained from the American Type Culture Collection (ATCC). Hep2, PK15, and *Spodoptera frugiperda* 9 (Sf9) cell lines were kept by our laboratory (39). Sf9 cells were cultured at 27°C in Grace's insect medium (pH 6.0; Gibco-BRL) supplemented with 10% fetal bovine serum (FBS; Gibco-BRL). HEK 293T, Hep2, HepG2, PK15, SH-SY5Y, and Vero cells were cultured at 37°C in Dulbecco's modified Eagle's medium (DMEM) (pH 7.0; Gibco-BRL) supplemented with 10% FBS. HeLa, HCM3, HEK 293, RD, and BHK-21 cells were cultured in Eagle's minimum essential medium (EMEM) (pH 7.0; Gibco-BRL) supplemented with 10% FBS. The recombinant virus Ac-BPegfp (6) and gp64-null AcBacmid (AcBacΔgp64) (40) were previously constructed in our laboratory. The recombinant virus VSV-GFP was a gift from Chunsheng Dong of Soochow University, China. The virus titer of recombinant AcMNPV was determined in Sf9 cells using an endpoint dilution assay, and TCID₅₀ was calculated.

Detection of virus binding. Cells were precooled on ice for 10 min and incubated with Ac-BPegfp at an MOI of 0.4, 5, or 20 TCID₅₀ units/cell for 1 h. The virus-containing medium was removed, the cells were washed with cold PBS 3 times to remove the unbound virus, and the cell-bound viral genome was quantified by qPCR with primers against the viral gene *vp80* as previously reported (39).

Detection of internalized virus particles. For direct-fusion pathway-mediated transduction, HeLa cells were treated with 20 nM BFA1 (Sigma-Aldrich) at 37°C for 30 min, chilled on ice, and incubated with Ac-BPegfp (MOI of 10 TCID₅₀ units/cell) at 4°C for 1 h. The virus-bound cells were collected to measure the total bound virions or treated with PBS (pH 4.8) for 5 min. After that, cells were cultured with DMEM containing BFA1 at 37°C for 1 h. Then, cells were digested by 0.05% (wt/vol) trypsin for 10 min, washed with PBS, and subjected to DNA extraction. For endocytosis pathway-mediated transduction, the protocol was similar to the direct-fusion-pathway-mediated transduction described above, except for the addition of BFA1 and PBS (pH 4.8) treatment. Viral-genome copies were detected as described above. For Sf9 cells, the experiment was performed similarly except for the culture temperature of 27°C.

Immunofluorescence microscopy. Cells were seeded onto coverslips and transduced with Ac-BPegfp (MOI of 200 TCID₅₀ units/cell) through the direct-fusion or endocytosis pathway as described above. Cells were fixed at 0, 1, 2, and 3 h p.t. (HeLa cells) or 0, 15, 30, and 60 min p.i. (Sf9 cells). Immunofluorescence microscopy was performed using anti-VP39 antibody and Alexa Fluor 488–goat anti-rabbit antibody (Abcam) as previously described (39). Cells were counterstained with Hoechst 33258 to stain the nuclei and imaged with a fluorescence microscope.

Fluorescence labeling of AcMNPV. Viruses were propagated, purified, and labeled with a self-quenching concentration (200 μM) of DiD as previously described (20, 41). Labeled virus was passed through Zeba spin desalting columns (Thermo Fisher Scientific) and a 0.45-μm filter to remove excess dye and aggregates, respectively, before being aliquoted and stored at –80°C until imaging. To label the virus with DiD and quantum dots (QDs) simultaneously, we followed a protocol established by Liu et al. (42).

Live-cell imaging. Live-cell imaging of virus infection was performed with a spinning-disk confocal microscope (UltraVIEW VoX) equipped with a cell culture system. Cells were transfected with plasmids expressing EGFP or mCherry-fused Rab5 or Rab7 for 24 h before infection with Ac-DiD. The prechilled dishes were incubated with the virus (MOI of 200 TCID₅₀ units/cell) on ice for 1 h and extensively washed before adding 2 ml cold culture medium. Samples were quickly mounted and brought into focus with the microscope to immediately acquire images. Next, the medium was replaced with prewarmed culture medium (37°C for mammalian cells or 27°C for insect cells) and images were acquired every 10 min.

Imaging analysis. The DiD intensity of each virus particle at each time point was calculated using ImageJ software (NIH). We set a level of 1.5-fold of the average fluorescence intensity of DiD at 0 min—beyond the maximal intensity at this time where no fusion occurred—as the threshold (I_t) to define a dequenched DiD particle. To calculate the colocalization of dequenched DiD and Rab5/7, dequenched DiDs were identified using ImageJ software by setting the threshold to I_t and overlaying the images with images of Rab5/7.

AcMNPV transduction of mammalian cells. For transduction of mammalian cells via the endocytosis pathway, cells were incubated with recombinant viruses at the MOIs indicated in Fig. 1A and 5C at 37°C for 1 h. Excess virus was then washed away, and cells were cultured for 24 h before flow cytometry (FCM) analysis. For transduction of mammalian cells via the direct-fusion pathway, cells were treated with 20 nM BFA1 to inhibit the endocytosis pathway and low pH (pH 4.8 or as indicated in Fig. 3B and 5F) was used to trigger AcMNPV transduction of mammalian cells by fusing with the cell membrane, as previously described (6).

Construction of recombinant bacmids containing mutated GP64. Recombinant AcMNPV containing the mutated or WT *gp64* gene and reporter *egfp* gene was generated according to the Bac-to-Bac baculovirus expression system protocol (Invitrogen). To generate the donor plasmid pFastBactTb-BPgp64^{WT}-BPegfp, the Op166-gp64-simian virus 40 (SV40) poly(A) cassette was cut out from pFB-Op166-gp64 (40) and subcloned downstream from the polyhedron gene promoter (P_{PH}) of the transfer vector pFastBactHTb, generating the pFastBactHTb-BPgp64^{WT} vector. The cytomegalovirus (CMV)-Op166-*egfp* cassette was cut out from pFastBactHTb-CMV-*egfp* (6) and inserted downstream from the Op166-gp64-SV40 poly(A) cassette of pFastBactHTb-BPgp64^{WT} to generate pFastBactHTb-BPgp64^{WT}-BPegfp. The sequence encoding site-directed mutagenesis of Asp to Glu in *gp64* was amplified by PCR and cloned into the pGEM-T easy vector (Promega) for sequencing. Next, the mutated *gp64* (*gp64*^{mutated}, including *gp64*^{D301E}, *gp64*^{D295E}, and *gp64*^{D295E/D301E}) genes were cut out and inserted into pFastBactHTb-BPegfp-BPgp64^{WT}, where the *gp64*^{WT} cassette was cut out by the same restriction enzymes, generating pFastBactHTb-BPegfp-BPgp64^{mutated}. The donor vectors were then transposed into the attTn7 integration

site of AcBac Δ gp64 (40). Finally, recombinant bacmids were screened via white-blue plaque selection and gentamicin resistance and identified by diagnostic PCR. The recombinant bacmids were named Ac Δ gp64-gp64^{WT}, Ac Δ gp64-gp64^{D295E}, Ac Δ gp64-gp64^{D301E}, and Ac Δ gp64-gp64^{D295E/D301E}.

Transfection and infection. Sf9 cells were transfected with each recombinant AcMNPV bacmid DNA, and the supernatants were collected 5 days posttransfection for an infection assay as previously described (43).

Detection of GP64 expression. Sf9 cells were infected with the recombinant viruses at an MOI of 5 TCID₅₀ units/cell for 48 h. The expression levels of GP64 were analyzed by Western blotting as previously reported (39). The cell surface display levels of GP64 were analyzed by cell surface enzyme-linked immunosorbent assay (cELISA) as described by Li and Blissard (44), using polyclonal anti-GP64 antibody (40).

Syncytium formation assays. Sf9 cells were infected with recombinant virus at an MOI of 5 TCID₅₀ units/cell for 48 h and triggered by low pH (pH 4.8 or as indicated in Fig. 3A) to form syncytia as described previously (45). Cell nuclei were stained with Hoechst 33258 and then imaged by fluorescence microscopy.

One-step growth curve analysis. The one-step growth curve experiment was performed as previously described (46). Briefly, Sf9 cells (1×10^6) were infected in triplicate with each recombinant virus in 6-well culture plates at an MOI of 5 TCID₅₀ units/cell for 1 h at 27°C. Then, the virus-containing medium was removed and cells were washed three times with Grace's insect medium before adding 2 ml fresh medium (Grace's insect medium with 10% FBS). Supernatants were collected at 0, 24, 48, and 72 h postinfection and clarified by centrifugation. Supernatant titers were determined by endpoint dilution assays to calculate TCID₅₀. Statistical significance analyses were performed using two-way analysis of variance (ANOVA) with GraphPad Prism (version 6.0; GraphPad Software, Inc.).

Alteration of endosomal pH. For inhibition of virus infection or transduction, cells were cultured for 30 min with BFA1 and NH₄Cl at the concentrations indicated in Fig. 6A to C or with dimethyl sulfoxide (DMSO) as control. The cells were then inoculated for 1 h with Ac-BPegfp at an MOI of 0.2 TCID₅₀ units/cell for Sf9 cells or 10 TCID₅₀ units/cell for HeLa cells in the presence of BFA1 and NH₄Cl. Next, the virus-containing culture medium was removed, and cells were washed and cultured in fresh medium containing BFA1 and NH₄Cl. Cells were cultured for another 4 h in the presence of BFA1 or NH₄Cl and then washed and cultured in fresh medium for 20 h before FCM analysis.

For inhibition of virus fusion, cells were cultured for 30 min with 20 nM BFA1 and 20 mM NH₄Cl or DMSO as control. The cells were then chilled on ice and incubated with Ac-DiD for 1 h. Unbound viruses were washed away before inhibitor-containing medium was added to the cells. After culturing for 1 h, the cells were immediately imaged.

Ouabain was used to enhance acidification of the EEs as described above for BFA1 and NH₄Cl. For virus transduction/infection, 0.8, 4, or 20 μ M ouabain was used and cells were transduced/infected by Ac-BPegfp at an MOI of 5 (mammalian cells) or 0.2 (Sf9) TCID₅₀ units/cell. For relative endosome pH measurements (described below), 0.8 μ M ouabain was used.

Endosomal pH measurement. To measure endosomal pH, we followed the protocol established by Wang et al. (26) with some modifications. HeLa cells were incubated with/without BFA1 or NH₄Cl for 30 min and loaded with 25 μ M LSYB in serum-free medium at 37°C for 5 min, washed twice, and immediately imaged at excitation/emission wavelengths of 390/435 nm (blue) and 390/525 nm (green). The green/blue ratio was calculated following the protocol established previously (47), and the pHs were calculated according to a calibration curve of green/blue ratios and pHs using methods previously described (47).

The relative comparison of endosomal pHs was performed by ratiometric fluorescence measurements as previously described (27). Briefly, cells were transfected with plasmids expressing Rab5^{mCherry} or Rab7^{mCherry} and incubated with a mixture of 5 mg/ml dextran conjugated to FITC (Sigma-Aldrich) and 60 μ g/ml dextran conjugated to Alexa Fluor 647 (Invitrogen) at 37°C for 20 min. Cells were washed extensively, after which the Rab5-labeled cells were imaged immediately, while the Rab7-labeled cells were cultured for another 20 min and then imaged. The fluorescence intensity ratio of FITC/Alexa-647 of each Rab5/7-positive endosome was analyzed by using ImageJ software.

ACKNOWLEDGMENTS

This work was supported by grants from the National Natural Science Foundation of China (grant no. 31621061 and 31370191) and the Strategic Priority Research Program of the Chinese Academy of Sciences (grant no. XDB11030400) and a grant to J.M.V. from the State Key Laboratory of Virology and the Wuhan Institute of Virology.

We thank Chunsheng Dong (Soochow University, China) for the generous gift of the virus VSV-GFP. We thank He Zhao, Li Li, Ding Gao, and Juan Min from the Core Facility and the Technical Support Facility of the Wuhan Institute of Virology for technical assistance.

REFERENCES

- Mansouri M, Berger P. 2018. Baculovirus for gene delivery to mammalian cells: past, present and future. *Plasmid* 98:1–7. <https://doi.org/10.1016/j.plasmid.2018.05.002>.
- Ono C, Okamoto T, Abe T, Matsuura Y. 2018. Baculovirus as a tool for gene delivery and gene therapy. *Viruses* 10:E5. <https://doi.org/10.3390/v10090510>.
- Blissard GW, Theilmann DA. 2018. Baculovirus entry and egress from insect cells. *Annu Rev Virol* 5:113–139. <https://doi.org/10.1146/annurev-virology-092917-043356>.
- Ohkawa T, Volkman LE, Welch MD. 2010. Actin-based motility drives baculovirus transit to the nucleus and cell surface. *J Cell Biol* 190:187–195. <https://doi.org/10.1083/jcb.201001162>.
- Long G, Pan X, Kormelink R, Vlak JM. 2006. Functional entry of baculovirus into insect and mammalian cells is dependent on clathrin-

- mediated endocytosis. *J Virol* 80:8830–8833. <https://doi.org/10.1128/JVI.00880-06>.
6. Dong S, Wang M, Qiu Z, Deng F, Vlak JM, Hu Z, Wang H. 2010. Autographa californica multicapsid nucleopolyhedrovirus efficiently infects Sf9 cells and transduces mammalian cells via direct fusion with the plasma membrane at low pH. *J Virol* 84:5351–5359. <https://doi.org/10.1128/JVI.02517-09>.
 7. Kataoka C, Kaname Y, Taguwa S, Abe T, Fukuhara T, Tani H, Moriishi K, Matsuura Y. 2012. Baculovirus GP64-mediated entry into mammalian cells. *J Virol* 86:2610–2620. <https://doi.org/10.1128/JVI.06704-11>.
 8. Laakkonen JP, Mäkelä AR, Kakkonen E, Turkki P, Kukkonen S, Peränen J, Ylä-Herttua S, Airene KJ, Oker-Blom C, Vihinen-Ranta M, Marjomäki V. 2009. Clathrin-independent entry of baculovirus triggers uptake of *E. coli* in non-phagocytic human cells. *PLoS One* 4:e5093. <https://doi.org/10.1371/journal.pone.0005093>.
 9. Wu C, Wang S. 2012. A pH-sensitive heparin-binding sequence from baculovirus gp64 protein is important for binding to mammalian cells but not to Sf9 insect cells. *J Virol* 86:484–491. <https://doi.org/10.1128/JVI.06357-11>.
 10. Liang C, Song J, Chen X. 2005. The GP64 protein of Autographa californica multiple nucleopolyhedrovirus rescues *Helicoverpa armigera* nucleopolyhedrovirus transduction in mammalian cells. *J Gen Virol* 86:1629–1635. <https://doi.org/10.1099/vir.0.80857-0>.
 11. Peng R, Zhang S, Cui Y, Shi Y, Gao F, Qi J. 2017. Structures of human-infecting thogotovirus fusogens support a common ancestor with insect baculovirus. *Proc Natl Acad Sci U S A* 114:E8905–E8912. <https://doi.org/10.1073/pnas.1706125114>.
 12. Blissard GW, Wenz JR. 1992. Baculovirus gp64 envelope glycoprotein is sufficient to mediate pH-dependent membrane fusion. *J Virol* 66:6829–6835.
 13. Kamiya K, Kobayashi J, Yoshimura T, Tsumoto K. 2010. Confocal microscopic observation of fusion between baculovirus budded virus envelopes and single giant unilamellar vesicles. *Biochim Biophys Acta* 1798:1625–1631. <https://doi.org/10.1016/j.bbammem.2010.05.011>.
 14. Pearson MN, Rohrmann GF. 2002. Transfer, incorporation, and substitution of envelope fusion proteins among members of the Baculoviridae, Orthomyxoviridae, and Metaviridae (insect retrovirus) families. *J Virol* 76:5301–5304. <https://doi.org/10.1128/JVI.76.11.5301-5304.2002>.
 15. Ojala K, Mottershead DG, Suokko A, Oker-Blom C. 2001. Specific binding of baculoviruses displaying gp64 fusion proteins to mammalian cells. *Biochem Biophys Res Commun* 284:777–784. <https://doi.org/10.1006/bbrc.2001.5048>.
 16. Makela AR, Matilainen H, White DJ, Ruoslahti E, Oker-Blom C. 2006. Enhanced baculovirus-mediated transduction of human cancer cells by tumor-homing peptides. *J Virol* 80:6603–6611. <https://doi.org/10.1128/JVI.00528-06>.
 17. Ge J, Huang Y, Hu X, Zhong J. 2007. A surface-modified baculovirus vector with improved gene delivery to B-lymphocytic cells. *J Biotechnol* 129:367–372. <https://doi.org/10.1016/j.jbiotec.2007.01.037>.
 18. Barsoum J, Brown R, McKee M, Boyce FM. 1997. Efficient transduction of mammalian cells by a recombinant baculovirus having the vesicular stomatitis virus G glycoprotein. *Hum Gene Ther* 8:2011–2018. <https://doi.org/10.1089/hum.1997.8.17-2011>.
 19. Borg J, Nevsten P, Wallenberg R, Stenstrom M, Cardell S, Falkenberg C, Holm C. 2004. Amino-terminal anchored surface display in insect cells and budded baculovirus using the amino-terminal end of neuraminidase. *J Biotechnol* 114:21–30. <https://doi.org/10.1016/j.jbiotec.2004.05.014>.
 20. Spence JS, Krause TB, Mittler E, Jangra RK, Chandran K. 2016. Direct visualization of Ebola virus fusion triggering in the endocytic pathway. *mBio* 7:e01857. <https://doi.org/10.1128/mBio.01857-15>.
 21. Katou Y, Yamada H, Ikeda M, Kobayashi M. 2010. A single amino acid substitution modulates low-pH-triggered membrane fusion of GP64 protein in Autographa californica and Bombyx mori nucleopolyhedroviruses. *Virology* 404:204–214. <https://doi.org/10.1016/j.virol.2010.04.028>.
 22. Yoshimori T, Yamamoto A, Moriyama Y, Futai M, Tashiro Y. 1991. Bafilomycin A1, a specific inhibitor of vacuolar-type H(+)-ATPase, inhibits acidification and protein degradation in lysosomes of cultured cells. *J Biol Chem* 266:17707–17712.
 23. Harada M, Sakisaka S, Yoshitake M, Kin M, Ohishi M, Shakado S, Mimura Y, Noguchi K, Sata M, Tanikawa K. 1996. Bafilomycin A1, a specific inhibitor of vacuolar-type H(+)-ATPases, inhibits the receptor-mediated endocytosis of asialoglycoproteins in isolated rat hepatocytes. *J Hepatol* 24:594–603. [https://doi.org/10.1016/S0168-8278\(96\)80146-2](https://doi.org/10.1016/S0168-8278(96)80146-2).
 24. Hefferon KL, Oomens AG, Monsma SA, Finnerty CM, Blissard GW. 1999. Host cell receptor binding by baculovirus GP64 and kinetics of virion entry. *Virology* 258:455–468. <https://doi.org/10.1006/viro.1999.9758>.
 25. Matos PM, Marin M, Ahn B, Lam W, Santos NC, Melikyan GB. 2013. Anionic lipids are required for vesicular stomatitis virus G protein-mediated single particle fusion with supported lipid bilayers. *J Biol Chem* 288:12416–12425. <https://doi.org/10.1074/jbc.M113.462028>.
 26. Wang C, Wang Y, Li Y, Bodemann B, Zhao T, Ma X, Huang G, Hu Z, DeBerardinis RJ, White MA, Gao J. 2015. A nanobuffer reporter library for fine-scale imaging and perturbation of endocytic organelles. *Nat Commun* 6:8524. <https://doi.org/10.1038/ncomms9524>.
 27. Feldmann T, Glukmann V, Medvenev E, Shpolansky U, Galili D, Lichtstein D, Rosen H. 2007. Role of endosomal Na⁺+K⁺-ATPase and cardiac steroids in the regulation of endocytosis. *Am J Physiol Cell Physiol* 293:C885–C896. <https://doi.org/10.1152/ajpcell.00602.2006>.
 28. Cain CC, Sipe DM, Murphy RF. 1989. Regulation of endocytic pH by the Na⁺,K⁺-ATPase in living cells. *Proc Natl Acad Sci U S A* 86:544–548. <https://doi.org/10.1073/pnas.86.2.544>.
 29. Kitajima M, Hamazaki H, Miyano-Kurosaki N, Takaku H. 2006. Characterization of baculovirus Autographa californica multiple nuclear polyhedrosis virus infection in mammalian cells. *Biochem Biophys Res Commun* 343:378–384. <https://doi.org/10.1016/j.bbrc.2006.02.167>.
 30. Liu Y, Joo KI, Lei Y, Wang P. 2014. Visualization of intracellular pathways of engineered baculovirus in mammalian cells. *Virus Res* 181:81–91. <https://doi.org/10.1016/j.virusres.2014.01.006>.
 31. Zaraket H, Bridges OA, Duan S, Baranovich T, Yoon SW, Reed ML, Salomon R, Webby RJ, Webster RG, Russell CJ. 2013. Increased acid stability of the hemagglutinin protein enhances H5N1 influenza virus growth in the upper respiratory tract but is insufficient for transmission in ferrets. *J Virol* 87:9911–9922. <https://doi.org/10.1128/JVI.01175-13>.
 32. Furuchi T, Aikawa K, Arai H, Inoue K. 1993. Bafilomycin A1, a specific inhibitor of vacuolar-type H(+)-ATPase, blocks lysosomal cholesterol trafficking in macrophages. *J Biol Chem* 268:27345–27348.
 33. Daidoji T, Watanabe Y, Ibrahim MS, Yasugi M, Maruyama H, Masuda T, Arai F, Ohba T, Honda A, Ikuta K, Nakaya T. 2015. Avian influenza virus infection of immortalized human respiratory epithelial cells depends upon a delicate balance between hemagglutinin acid stability and endosomal pH. *J Biol Chem* 290:10627–10642. <https://doi.org/10.1074/jbc.M114.611327>.
 34. Fujita R, Matsuyama T, Yamagishi J, Sahara K, Asano S, Bando H. 2006. Expression of Autographa californica multiple nucleopolyhedrovirus genes in mammalian cells and upregulation of the host beta-actin gene. *J Virol* 80:2390–2395. <https://doi.org/10.1128/JVI.80.5.2390-2395.2006>.
 35. Portela A, Jones LD, Nuttall P. 1992. Identification of viral structural polypeptides of Thogoto virus (a tick-borne orthomyxo-like virus) and functions associated with the glycoprotein. *J Gen Virol* 73(Pt 11):2823–2830. <https://doi.org/10.1099/0022-1317-73-11-2823>.
 36. Bissig C, Johnson S, Gruenberg J. 2012. Studying lipids involved in the endosomal pathway. *Methods Cell Biol* 108:19–46. <https://doi.org/10.1016/B978-0-12-386487-1.00002-X>.
 37. Kielian MC, Helenius A. 1984. Role of cholesterol in fusion of Semliki Forest virus with membranes. *J Virol* 52:281–283.
 38. Zaitseva E, Yang ST, Melikov K, Pourmal S, Chernomordik LV. 2010. Dengue virus ensures its fusion in late endosomes using compartment-specific lipids. *PLoS Pathog* 6:e1001131. <https://doi.org/10.1371/journal.ppat.1001131>.
 39. Li Y, Shen S, Hu L, Deng F, Vlak JM, Hu Z, Wang H, Wang M. 2018. The functional oligomeric state of tegument protein GP41 is essential for baculovirus budded virion and occlusion-derived virion assembly. *J Virol* 92:e02083-17.
 40. Wang M, Tan Y, Yin F, Deng F, Vlak JM, Hu Z, Wang H. 2008. The F-like protein Ac23 enhances the infectivity of the budded virus of gp64-null Autographa californica multinucleocapsid nucleopolyhedrovirus pseudotyped with baculovirus envelope fusion protein F. *J Virol* 82:9800–9804. <https://doi.org/10.1128/JVI.00759-08>.
 41. Wang R, Deng F, Hou D, Zhao Y, Guo L, Wang H, Hu Z. 2010. Proteomics of the Autographa californica nucleopolyhedrovirus budded virions. *J Virol* 84:7233–7242. <https://doi.org/10.1128/JVI.00040-10>.
 42. Liu J, Xu M, Tang B, Hu L, Deng F, Wang H, Pang DW, Hu Z, Wang M, Zhou Y. 2019. Single-particle tracking reveals the sequential entry process of the bunyavirus severe fever with thrombocytopenia syndrome virus. *Small* 2019:e1803788. <https://doi.org/10.1002/sml.201803788>.
 43. Wang M, Shen S, Wang H, Hu Z, Becnel J, Vlak JM. 2017. Deltabaculo-

- viruses encode a functional type I budded virus envelope fusion protein. *J Gen Virol* 98:847–852. <https://doi.org/10.1099/jgv.0.000745>.
44. Li Z, Blissard GW. 2011. *Autographa californica* multiple nucleopolyhedrovirus GP64 protein: roles of histidine residues in triggering membrane fusion and fusion pore expansion. *J Virol* 85:12492–12504. <https://doi.org/10.1128/JVI.05153-11>.
45. Zou Z, Liu J, Wang Z, Deng F, Wang H, Hu Z, Wang M, Zhang T. 2016. Characterization of two monoclonal antibodies, 38F10 and 44D11, against the major envelope fusion protein of *Helicoverpa armigera* nucleopolyhedrovirus. *Viol Sin* 31:490–499. <https://doi.org/10.1007/s12250-016-3831-4>.
46. Makalliwa GA, Wang X, Zhang H, Zhang N, Chen C, Li J, Deng F, Wang H, Wang M, Hu Z. 2018. *HearNPV* pseudotyped with PIF1, 2, and 3 from *MabrNPV*: infectivity and complex stability. *Viol Sin* 33:187–196. <https://doi.org/10.1007/s12250-018-0014-5>.
47. Diwu Z, Chen CS, Zhang C, Klaubert DH, Haugland RP. 1999. A novel acidotropic pH indicator and its potential application in labeling acidic organelles of live cells. *Chem Biol* 6:411–418. [https://doi.org/10.1016/S1074-5521\(99\)80059-3](https://doi.org/10.1016/S1074-5521(99)80059-3).
48. Kadlec J, Loureiro S, Abrescia NG, Stuart DI, Jones IM. 2008. The post-fusion structure of baculovirus gp64 supports a unified view of viral fusion machines. *Nat Struct Mol Biol* 15:1024–1030. <https://doi.org/10.1038/nsmb.1484>.